Stability of X-Bracing Systems with Traditional Bolted Connections

R. Tremblay[1], A. Davaran[1] and A. Gélinas[1]

[1]Group for Research in Structural Engineering, Department of Civil, Geological and Mining Engineering, Ecole Polytechnique, Montreal, QC, Canada, H3C 3A7.
email: robert.tremblay@polymtl.ca

ABSTRACT

This paper deals with the design for stability of steel concentrically X-bracing frames built with HSS bracing members. Traditional slotted-tube connections with bolted shear splices are used for the bracing members. Both single- and double-shear splices are investigated. Full-scale quasi-static cyclic test program showed that instability of the discontinuous braces initiated through bending deformations of the connection plates, prior to overall buckling of the bracing members. Elastic stability analysis is performed to assess the effective buckling length and compressive resistances of the bracing members with double shear connections. Brace resistances are also obtained from an analytical model that accounts for inelasticity effects and geometrical imperfections of the brace connections. Numerical predictions are compared to test results and a numerical example is included to illustrate the method.

INTRODUCTION

HSS tubular bracing members arranged in an X-bracing configuration is one of the common bracing design options for building and industrial structures. The possibility of using a reduced effective length factor, typically K = 0.5, for the compression braces and the resulting smaller member sizes make this system attractive to design engineers. The key issue in the stability of the compression brace in an X-bracing is the in-plane and out-of-plane restraint provided by the intersecting member acting in tension. In earlier analytical work on the stability of this system (e.g., DeWolf and Pelliccione, 1979; Picard and Beaulieu, 1987), bracing members were assumed to have pinned end connections and uniform flexural stiffness properties over their full length. Stoman (1989) and Segal et al. (1994) examined the influence of using fixed and semi-rigid end connections. Studies by Davaran (2001) and Davaran and Hoveidae (2009) showed that the reduction of the flexural stiffness of the tension brace due to the presence of connection plates at the mid-connection can reduce the strength of the compression brace. Cyclic tests by Tremblay et al. (2003) indicated that a K factor of 0.5 can be used for out-of-plane buckling of HSS braces in X-braced frames when welded cover plates are used at the mid-connection to provide for flexural continuity of the cut brace.

In practice, X-bracing with slotted-HSS bolted plate connections are more commonly used. The connections can be detailed with single-shear (SS) lap splices or double-shear (DS) lap splices (Figure 1). The former type is simpler and easier to assemble in the field. However, it is unsymmetrical and has inherent out-of-plane eccentricity. Double shear connections are symmetrical (no eccentricity) and are typically shorter as fewer bolts are needed. Fabrication and assembly on site of DS connections are generally more difficult.

a) b)

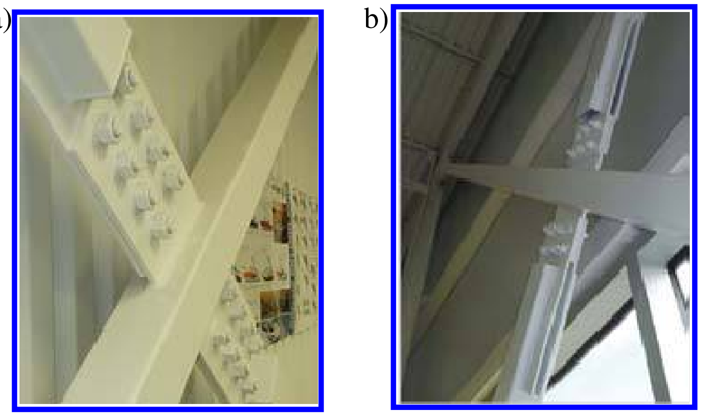

Figure 1. Connections at brace intersection in X-bracing:
a) Single shear bolted lap splices (SS); b) Double shear bolted lap splices (DS).

In a recent quasi-static cyclic test program (Gélinas et. al., 2012; Davaran et. al., 2012), the stability of full-scale X-bracing specimens with details similar to those shown in Figure 1 was investigated. The tests revealed that instability of the discontinuous brace was initiated by flexural out-of-plane deformations of the connecting plates. Buckling modes involving plastic hinges forming in the connecting plates eventually formed without flexural deformations of the HSS members between the hinges (Figure 2). The compressive strengths associated to such buckling modes were lower than the expected brace compressive resistances.

Figure 2. Connection instability observed in the tested specimens.

This paper investigates the stability of the discontinuous brace in steel X-braced frames built with HSS bracing members with bolted slotted connections. Experimental observations for the specimens with SS and DS connections are first reported. An analytical method is proposed to assess the effective length of discontinuous braces with DS connections including connection flexibility effects. The method is used to predict the values obtained by tests. In the last section of the paper, a design example is presented to illustrate the application of the method.

EXPERIMENTAL OBSERVATIONS

Description of the test specimens. The stability response of 11 X-bracing specimens subjected to quasi-static cyclic displacement is examined in this paper. The test frame was 7.5 m wide x 4.087 m high. The beams were connected to the columns using simple shear connections and lateral loads were essentially resisted by the bracing members. All bracing members were made of ASTM A500, gr. C square tubing. Three specimens were detailed with SS splice connections whereas DS connections were used for the remaining ones.

The geometrical characteristics of the two mid-connection types are depicted in Figure 3 and the measured properties are summarised in Tables 1 and 2, respectively. In all specimens, a middle plate was inserted though the continuous HSS brace and the plates inserted in slots at the ends of the discontinuous HSS brace segments were connected to that middle plate using the SS and DS bolted shear splice connections. In Table 3, the free distances left at the end of the overlapping plates in the splice connections are given. The length g_2 is the free length between the end of the HSS member and the gusset plate at the corner connections.

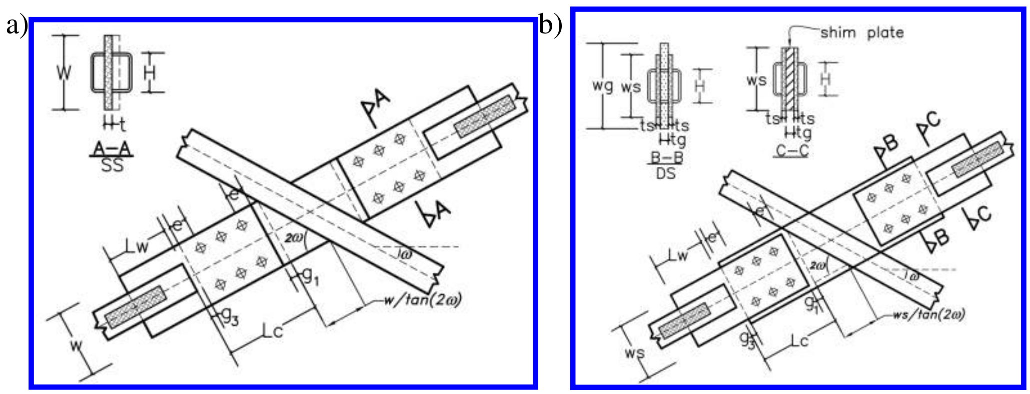

Figure 3. Typical mid-connection details:
a) SS connection, and b) DS splice connection.

Table 1. Characteristics of the specimens with SS connections

No	HSS Size	L (mm)	L_c (mm)	t (mm)	w (mm)	F_y (MPa)	P_{Test} (kN)
7	127X127X7.9	3105	389	16.48	280	378	454
8	127X127X7.9	3130	406	25.58	200	372	535
14	102x102x6.4	3162	232	16.52	152.4	378	284

Table 2. Characteristics of the specimens with DS connections

No	HSS Size	L (mm)	L_c (mm)	t_g (mm)	t_s (mm)	w_g ,w_S (mm)	F_y (MPa)	P_{Test} (kN)
1	127X127X7.9	3097	388	19.05	9.525	304.8	408	751
2	127X127X7.9	3097	428	19.05	9.525	304.8	408	834
5	127X127X7.9	3111	307	16.3	8.15	260	387	677
6	127X127X7.9	3124	307	19.12	9.56	220	408	847
10	127X127X7.9	3137	232	16.08	8.04	180	387	586
11	127X127X7.9	3137	240	9.73	8.01	320	410	474
12	102x102x6.4	3133	307	16.4	8.2	240	387	477
13	102x102x6.4	3161	203	16.54	8.27	152.4	387	433

In specimens with DS connections, a clear distance is left between the two splice plates inserted at the HSS member ends. In practice, this opening can be filled with a shim plate having the same thickness as the middle plate, as illustrated in Figure 3b. In the test program, no shim plate was used for Specimen no. 13. Specimens nos. 10 and 12 had shim plates attached to the splice plates by a few tack welds. For the remaining specimens with DS connections, pairs of parallel continuous structural welds were used to connect the shim plates to the splice plates.

Table 3. Free distances left between connecting plates.

Connection Type	No.	g_1 (mm)	g_2 (mm)	g_3 (mm)	e (mm)	K_c
SS	7	32	32	25	71	-
	8	49	49	25	71	-
	14	32	32	25	50	-
DS	1	40	40	25	50	1.55
	2	80	40	25	50	1.48
	5	32	32	25	50	1.81
	6	32	40	25	50	1.78
	10	32	32	25	50	2.16
	11	40	40	25	50	1.95
	12	32	32	25	50	1.77
	13	32	32	25	36	2.12

Observed stability response. Buckling of the discontinuous braces is examined herein. Buckling occurred out-of-plane for all specimens. The measured out-of-plane deformations at the time just before reaching peak compression load producing buckling of the discontinuous brace are illustrated in Figure 4 (amplified by 10). In the figure, the cross-section of the continuous brace is schematically illustrated at the brace intersecting point (node 5). These deformed shapes near buckling can be seen as combinations of the three basic modes *M0*, *M1* and *M2* depicted in Figure 5.

In all specimens, global lateral deformation mode *M0* took place during the small amplitude, elastic frame lateral displacement cycles, before buckling of the discontinuous brace occurred. Out-of-plane deformations at the brace intersecting point (node 5 in Figure 5), were maximum when compression was induced in the discontinuous brace, just after crossing the zero displacement position of the frame. As tension load increased in the continuous brace, out-of-plane deformations at node 5 eventually stopped increasing and reduced as the lateral support provided by the tension brace gained stiffness. As shown in Figure 4, when approaching the peak compression force, the discontinuous braces laterally deformed following essentially mode *M1* or mode *M2*. In either case, the buckling mode included some global lateral deformation following *M0* but the continuous bracing member served as a support preventing/limiting the lateral and torsional movements of the brace intersection point. Prevalence between *M1* and *M2* modes depends on several factors, including the flexural stiffness of the connecting plates, inherent eccentricity for the SS connections, and torsional stiffness of the continuous member.

For the specimens with SS connections (nos. 7, 8 and 14), buckling took place mainly along mode *M1*, i.e., with out-of-plane deformations concentrating in only one segment of the discontinuous member and no, or limited torsional rotation of the continuous brace. Upon buckling, flexural deformations concentrated in the free distance g_1 next to the continuous brace, the free distance g_3 at the end of the splice overlap, and in the free distance g_2 at the corner connection, at the opposite end of the HSS member segment. Plastic hinging developed first in the gap distance g_3, followed, in the post-buckling range, by a second plastic hinge in gap g_1 and further rotation in gap g_2 to form a three-hinge mechanism. This *M1* buckling mode is illustrated in Figure 6a for Specimen no. 7.

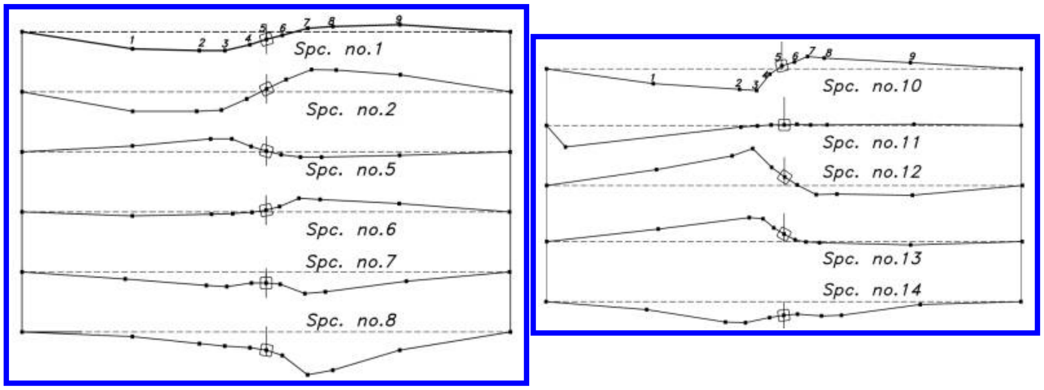

Figure 4. Out-of-plane deformations of the discontinuous brace just before peak compression load producing buckling.

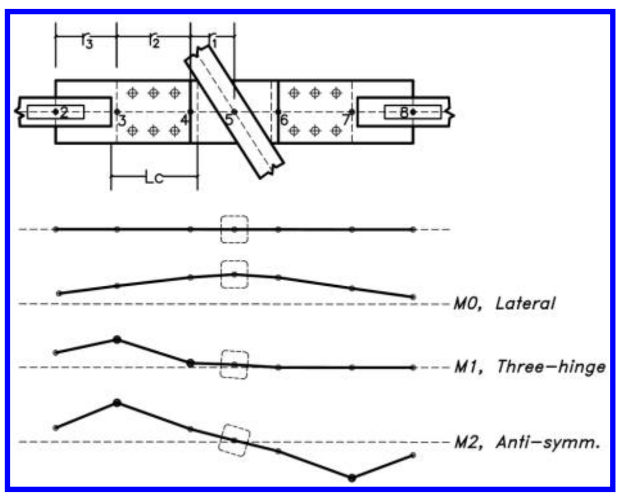

Figure 5. Buckling modes observed in the tests.

For the specimens with DS connections, the discontinuous brace exhibited out-of-plane deformations closer to *M2* for most specimens, i.e., with out-of-plane anti-symmetrical deformation of the discontinuous brace developing in the opposite directions on either side of the continuous brace. Again, this deformation pattern is the result of bending of the connecting plates in the free distances g_1 to g_3. This time, however, it is accompanied with more pronounced torsional rotation of the continuous brace. Deformation mode *M2* is illustrated in Figure 6b for the discontinuous brace of Specimen no. 1. Upon buckling, flexural yielding developed in free distance g_3, followed by plastic hinge in distance g_1. A third flexural hinge then developed in the HSS segments near the tip of the slots created for inserting the splice plates (Figure

6c). Specimen no. 2 also deformed according to *M2* mode (Figure 4). As illustrated in Figure 6d, inelastic deformations after buckling concentrated on only one side of the continuous brace.

Local bending deformations of the slotted HSS at the end of the discontinuous brace segments took place at buckling of the braces, as illustrated in Figure 7. The presence of the slotted holes, the absence or presence of shim plates, and the degree of attachment of the shim plates to the splice plates are factors that likely affected the flexural stiffness of the mid-connections and, thereby, the buckling strength of the discontinuous braces. This will be discussed when analyzing the tests results.

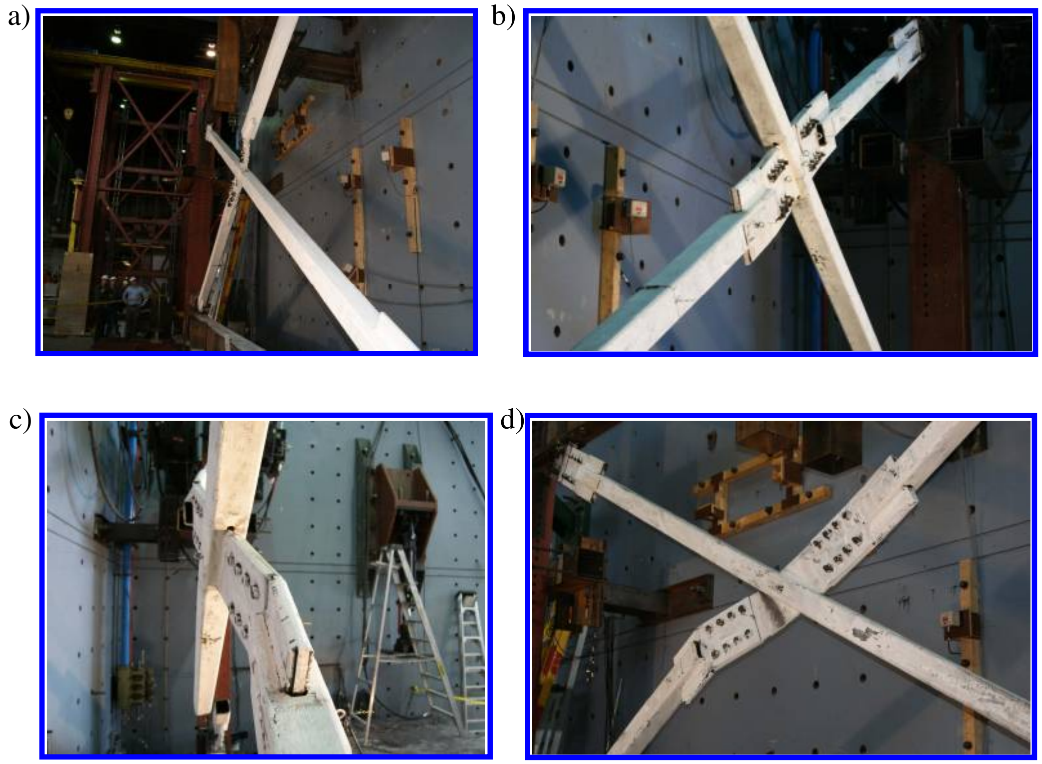

Figure 6. Deformed discontinuous brace in specimens with: a) SS connections (Mode *M1*, Specimen no. 8); b) & c) DS connections (Mode *M2*, Specimen No. 1); and d) DS connections (Mode *M1*, Specimen no. 2).

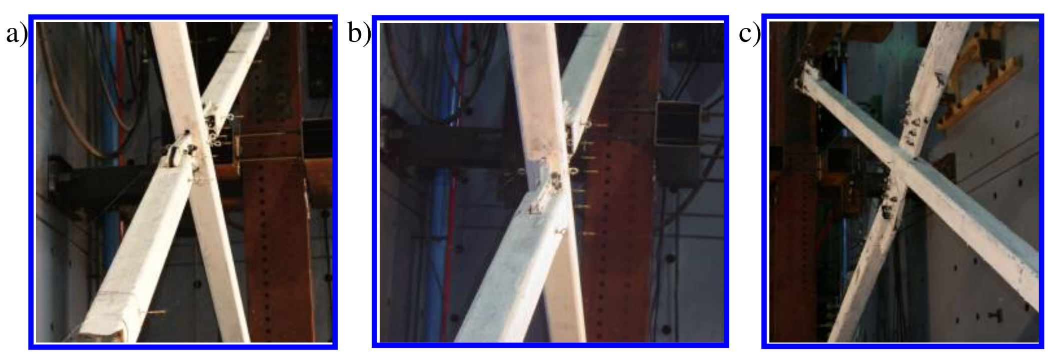

Figure 7. Deformed discontinuous brace in specimens with DS connections: a) Without shim plates (Specimen no. 13); b) With tacked shim plates (Specimen no. 10); and c) With continuously welded shim plates (Specimen no. 5).

Buckling modes for the discontinuous brace can also be examined by looking at the axial load *vs* connection rotations in the quarter cycle when buckling occurred. In Figure 8, the rotation of segments r_1 and r_2 in Figure 5 are used to reflect the connection rotation. These rotations are calculated on the left- and right-hand sides of the continuous brace:

$$\theta_L = \frac{d_5 - d_4}{r_1}, \quad \theta_R = \frac{d_6 - d_5}{r_1} \tag{1}$$

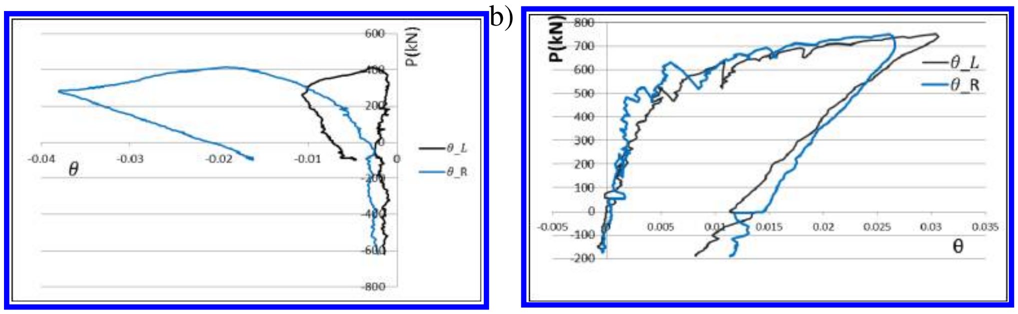

Figure 8. Axial load *vs* connection rotation response at buckling of the discontinuous brace in: a) Specimen no. 7 (mode *M1*); and b) Specimen no. 1 (mode *M2*).

For Specimen no. 7 with SS connections in Figure 8a, the rotation essentially developed on one side of the one side of the mid-connection prior to buckling, confirming *M1* behavior. In the post-buckling range, the rotation developed further along the same mode. In Specimen no. 1 in Figure 8b, buckling of the discontinuous brace occurred at the very end of a frame displacement cycle. Contrary to Specimen no. 7, very similar rotation responses were recorded on either side of the continuous brace, confirming mode *M2*. In that mode, the whole mid-connection rotates and torsional stiffness of the continuous brace is engaged.

CURRENT DESIGN METHOD

Design method. The AISC steel design guide no. 24 (AISC, 2010) provides a design method that directly addresses the stability of a SS connection for HSS members. The model assumed in the guide is illustrated in Figure 9a. No such established method exists in codes or design guides for DS connections. In this section, the compressive resistances of the discontinuous braces, P_{Test}, as measured in the tests and given in Tables 1 and 2 are compared to the predictions from the method given in the AISC guide. For this purpose, the connection is modelled as shown in Figure 9b and assumptions in the AISC guide for SS connections are adopted for the DS connections.

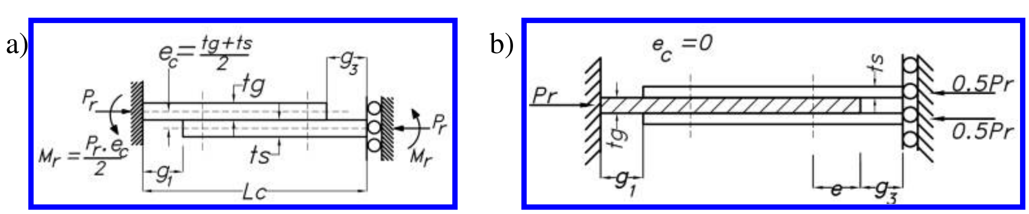

Figure 9. Simplified models for: a) SS connections; b) DS connections.

For SS connections, the resistance is obtained using the interaction equation for combined flexure and compression from the AISC Specification (AISC 2010):

$$(2)\qquad \begin{aligned} &\frac{P_r}{P_c}+\frac{8}{9}\left(\frac{M_r}{M_c}\right)\leq 1.0 \qquad && \text{for } \frac{P_r}{P_c}\geq 0.2 \\ &\frac{P_r}{2P_c}+\frac{M_r}{M_c}\leq 1.0 \qquad && \text{for } \frac{P_r}{P_c}< 0.2 \end{aligned}$$

where P_c and M_c are the available strengths of the single plate in axial compression and flexure, respectively, as also determined from the Specification. The strength P_c is calculated with an effective length K_cL_c, where K_c = 1.2 and L_c is the length of the connection, and with the cross-section properties of the thinner of the two overlapping plates. In Figure 9a, lengths g_1 and g_3 are indicated for reference to the mid-connection detail of Figure 3a. From equilibrium, the moment $M_r = P_r \cdot e_c/2$. The connection axial resistance P_r is taken as the minimum P_r value obtained by solving the two expressions in Eq. (1).

For DS connections, the eccentricity $e_c = 0$ and the connection resistance P_r is taken equal to the available strength P_c determined with the K_cL_c value used for SS connections. According to the AISC guide, P_c should also be determined based on the properties of the thinner cross-section. In Figure 9b, either the single plate with thickness t_g or the section with two plates of thickness t_s separated by the clear distance t_g could be considered. For the second case, the moment of inertia, I_s, is given by:

$$(3)\qquad I_s = 2\left(\frac{w_s t_s^3}{12}\right)+\rho\left(2w_s t_s\right)\left(\frac{t_s+t_g}{2}\right)^2$$

where ρ is a factor that accounts for the degree of composite action between the two plates. For the comparison, the calculations are performed for both cross-sections but preference will be given to the results obtained for the second (composite) one because the tests clearly showed that buckling of the discontinuous brace occurred when flexural yielding initiated in the free distance g_3. In Eq. (3), a conservative value $\rho = 0$ is assumed for this calculation, assuming that no, or limited composite action develops between the two splice plates. Observation in tests showed that the two plates exhibited individual response in the post-buckling range (Figure 10), suggesting that this assumption could be appropriate for determining the buckling resistance.

Comparison with test results. The predicted resistances are compared to the test results in Figure 11. For SS connections, the P_r values are generally close (within 15%) to the measured values but, for two specimens, the predictions are on the non conservative side. For the DS cases, the figure shows that large differences exist depending on the cross-section adopted in the calculations. When using the single plate (t_g) corresponding to the free length g_1, the resistances are generally overestimated with predicted-to-test ratios varying between 1.08 and 1.84. Lower values are found when using the cross-section corresponding to the double splice plates ($2t_s$). In that case, the test-to-predicted ratios range from 0.31 to 0.91, indicate that the approach would be very conservative. The deviations from the measured values for the DS connections are significantly greater than for the SS connections.

Figure 10. Deformation of double splicing plates at plastic hinge node 3 or 7.

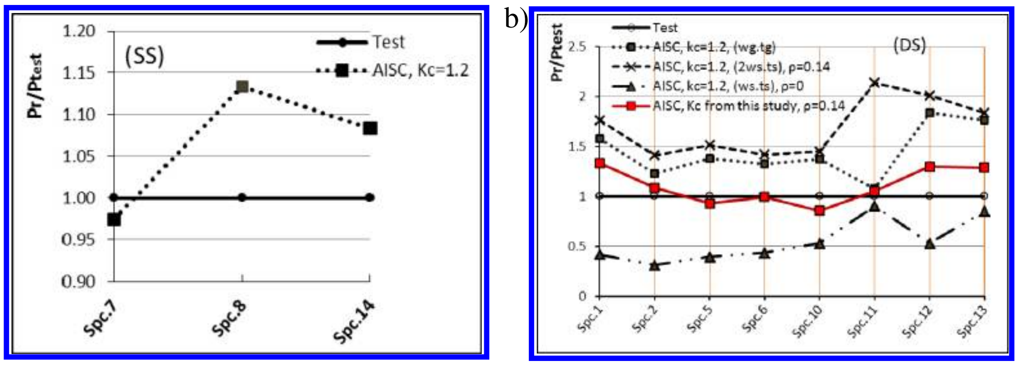

Figure 11. Comparison between predicted axial resistances and test results for specimens with: a) SS connections; b) DS connections.

PROPOSED DESIGN METHOD FOR DS CONNECTIONS

Elastic buckling analysis. In this section, elastic buckling analysis is performed to determine the elastic buckling load and the corresponding effective length factor for DS connections. A model is developed assuming that the discontinuous bracing member and the overlapping length of the plates remained do not deform in bending at buckling and that out-of-plane displacements are only produced by the bending of the connecting plates in the free lengths, g_1 to g_3, as was observed in tests. The model is shown in Figure 12. The flexural stiffness of the connecting plates is represented by rotational springs located at connection ends (denoted by nodes 3, 4, 6 and 7 in Figure 4).

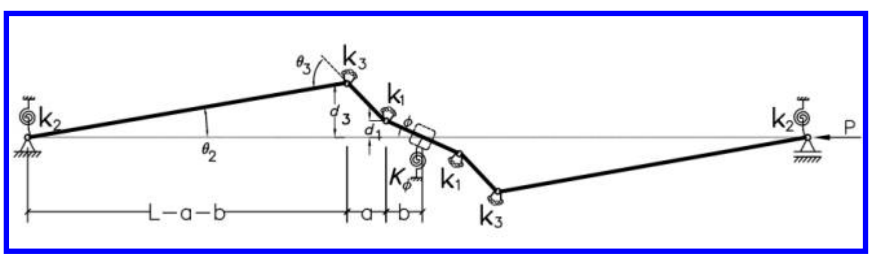

Figure 12. Model for prediction buckling of the DS connection.

The rotational stiffness of the springs can be defined by the properties of the connected plates as $k_i = EI_i / \overline{g}_i$, where $\overline{g}_i$ is the equivalent length of the plate segments involved in bending. For the segment g_1, elastic finite element analysis of the flexural response of the middle plate connecting at an angle ω to the continuous brace (see Figure 3b) was performed to determine $\overline{g}_1$. For segment g_3, the length was increased by the end distance e whereas no modification was needed for the segment g_2:

$$\overline{g}_1 = g_1 + \tau\left(\frac{90-2\omega}{40}\right)^{0.625} \qquad (4)$$
$$\overline{g}_2 = g_2$$
$$\overline{g}_3 = g_3 + e$$

In Eq. (4) the parameter τ = 0.87t and 1.43t for plate width-to-thickness ratios w/t = 10 and 20, respectively. Linear interpolation is used for intermediate w/t values. For spring k_3, the flexural stiffness is determined using the moment of inertia I_s from Eq. (3). This time, an intermediate value ρ = 0.14 is selected, as justified from test results and discussed in the next section. Finally, the torsional stiffness of the continuous brace is obtained from:

$$k_\varphi = \frac{2GJ}{L.Sin^2(2\omega)}\eta \quad \text{, where: } \eta = \frac{1}{3}\frac{(\lambda L)^3}{\lambda L - \tanh(\lambda L)} \text{ with } \lambda L = \pi\sqrt{\frac{T}{P_e}} \qquad (5)$$

where η is a tensile stiffening parameter that magnifies the initial torsional stiffness due to tension load T in the continuous brace (Davaran, 2001). Based on these assumptions, assuming a perfectly anti-symmetrical buckling mode, the deformed shape at buckling of the model in Figure 12 can be entirely defined by the two degrees of freedom d_1 and d_3 and static equilibrium in the deformed position yields:

$$\overline{\mathbf{K}}\ \mathbf{d} = \mathbf{0} \qquad (6)$$

where $\overline{\mathbf{K}}$ is the stiffness matrix of the system including nonlinear geometric effects:

$$k_{11} = \frac{1}{L}\left(-\frac{k_3}{L\gamma_1} + \frac{k_\varphi}{2}\frac{(1-\gamma_1-\gamma_2)}{L\gamma_2}\right);$$
$$k_{13} = \frac{1}{L}\left(k_2\frac{(\gamma_1+\gamma_2)}{L(1-\gamma_1-\gamma_2)} + k_3\frac{(1-\gamma_2)}{L\gamma_1(1-\gamma_1-\gamma_2)} - P\right) \qquad (7)$$
$$k_{31} = \frac{1}{L}\left(k_1\frac{(\gamma_1+\gamma_2)}{L\gamma_1\gamma_2} + \frac{k_\varphi}{2}\frac{(1-\gamma_2)}{L\gamma_2} - P\right);\ k_{33} = \frac{1}{L}\left(k_2\frac{\gamma_2}{L(1-\gamma_1-\gamma_2)} - \frac{k_1}{L\gamma_1}\right)$$

In these expression, $\gamma_1 = a/L$ and $\gamma_2 = b/L$ (see Figure 12 for dimensions a and b). By setting the determinant of that matrix equal to zero, the following quadratic equation is obtained :

$$P^2 - c.P + d = 0 \quad \text{, where: } c = k_{13} + k_{31};\quad d = k_{13}.k_{31} - k_{11}.k_{33} \qquad (8)$$

The elastic buckling load P_{cr} is the smaller of the two roots obtained from this quadratic equation. After calculating, P_{cr}, the effective length with respect to connection can be evaluated by the following relations

$$K_c = \sqrt{\frac{P_{e,c}}{P_{cr}}} \quad , \text{ with } P_{e,c} = \frac{\pi^2 EI_s}{L_c^2} \tag{9}$$

Comparison with test results. As was done in the previous section, the effective length K_cL_c is used to determine the compressive resistance P_r from the AISC Specification. In that calculation, it is proposed to use the cross-section properties of the double splice plates ($2t_s$) because it corresponds to the gap segment g_3 where yielding triggering buckling of the discontinuous brace assembly was observed in the tests. For consistency, the load P_{ec} in Eq. (9) is also determined using the moment of inertia I_s. In Eq. (3) for I_s, the factor ρ was used to account for imperfect composite action. Here, it proposed to use that factors to account for various elements affecting the flexural stiffness of the splice plates such as: relative longitudinal slip between bolted plates, local deformations of the splicing plates over the length g_3, local buckling of unsupported splice plates, inelasticity and initial imperfection effects, and absence or improper connection of shim plates. By trial and errors, a value $\rho = 0.14$ was determined to obtain reasonable match between test and predicted strength values. As shown in Figure 11b, excellent correspondence is achieved for Specimens nos. 2, 5, 6, 10 and 11 with this ρ value. The method however over-predicts the resistance of Specimens nos. 1, 12 and 13. For the former, the difference can be attributed to the more pronounced bolt slip response observed in this test, as evidenced by the fluctuations in the response of Figure 8b. Specimens 12 and 13 were detailed with tacked shim plates and without shim plates, respectively, which may have reduced their capacities. Further investigation (numerical simulations) are needed to better characterize these affecting factors and confirm the use of the r factor to account for these effects. Meanwhile, based on available data, using $\rho = 0.14$ seems to be appropriate. Using this value, the calculated effective length factors K_c vary between 1.48 to 2.16, as shown in Table 3. this value is value is higher than the 1.2 factor from current design methods. In igure 11b, it is seen that using $\rho = 0.14$ with $K_c = 1.2$ significantly overestimates the compressive strength of all braces.

DESIGN EXAMPLE

The mid-connection of an X-bracing with DS connections is to be designed to resist a force corresponding to expected ultimate capacity of the bracing member. The braced frame has a span of 7620 mm and a height of 3962 mm. The braces are ASTM A500, gr. C, HSS152x152x6.4 with A = 3380 mm^2, r = 59.4 mm, J = 40411 mm^4, F_y = 345 MPa, F_u = 427 MPa and expected yield strength, F_{ye} = 490 MPa. Connecting plates are ASTM A572 steel with F_{yp} = 345 MPa, F_{up} = 448 MPa. The connections done with pre-tensioned A490 bolts and E70XX electrodes. Continuously welded shim plates are used between the splice plates.

The expected brace tensile strength is obtained from $T_{exp} = AF_{ye}$ = 1656 kN. For the brace compressive resistance, a buckling length equal to 0.8 times the center length dimension is used, which results in $P_{exp} = 1.14A_gF_{cre}$ = 1334 kN. The torsional stiffness of the continuous HSS is k_ϕ = 6464 kN-mm/rad. A trial design connection satisfying all the code tension strength requirements is developed, which give preliminary plate thickness and widths. Plate dimensions from this first design trial are given in Table 4. The connection has 2 rows of three 22.2 mm bolts spaced 70 mm o/c. An edge distance e = 40 mm and the free lengths are: $g_1 = g_2 = 44.5$ mm and $g_3 = 25.4$ mm. The corresponding modified lengths are $\overline{g}_1 = 73.77$ mm and $\overline{g}_3 = 65.4$ mm. From geometry, $a = L_c = 290$ mm and $b = 189$ mm, which gives $\gamma_1 = 0.08437$ and $\gamma_2 = 0.054902$. For this first trial, stiffness $k_1 = 677\text{x}10^3$ kN-mm/rad. Assuming $\rho = 0.14$, $k_3 = 913\text{x}10^3$ kN-mm/rad. For simplicity, for the calculation of k_2, the corner gusset plates are assumed to have the same dimensions as the middle plate. As will be discussed, the dimensions assumed for k_2 have little influence on the buckling strength of the discontinuous brace.

In Table 4, three values of resistances are computed for each trial: one considering k_2 and T = 0.5 P_{exp}, one with $k_2 = 0$ and T = 0.5 P_{exp} and one with $k_2 = T = 0$. For the first trial design, the factored resistance ($\phi = 0.9$) is equal to 1149 kN, which is less than the required design strength of 1334 kN. As shown, ignoring k_2 in the calculations has nearly no effect because this rotational restraint is located far from the mid-connection. Similarly, for this example, the stiffening effect of T on the torsional restraint provided by the continuous brace also has negligible impact on the stability of the discontinuous brace. To increase of the strength of the discontinuous brace, the thickness of the splice plates is increased from 11.1 mm to 12.7 mm. This change increases the stiffness k_3 to $1190\text{x}10^3$ kN-mm/rad and, as shown in Table 4, it is sufficient to achieve the required compressive resistance of 1336 kN. It is noted that in all cases, the K_c factor is close to 2.0, which is larger than 1.2.

Table 4. Designed gusset plates and connection buckling capacity.

Trial No.	t_g (mm)	t_s (mm)	w_g, w_s (mm)	k_2 (kN-mm/rad)	T (kN)	P_{cr} (kN)	K_c	ϕP_c (kN)
1	22.225	11.113	273	$1124\text{x}10^3$	0.5 P_{exp}	1771	1.99	1149
				0	0.5 P_{exp}	1723	2.02	1133
				0		1717	2.02	1131
2	22.225	12.7	273	$1124\text{x}10^3$	0.5 P_{exp}	2098	2.09	1336
				0	0.5 P_{exp}	2052	2.11	1322
				0	0	2045	2.11	1321

CONCLUSIONS

The response of 11 quasi-static cyclic tests on steel X-braced frames with HSS-slotted bolted connections was examined to study the stability response of the discontinuous bracing members. The compressive strength and buckling mode of the discontinuous braces was influenced by local bending deformations of the connecting plates at the mid-connections and, to a lesser extent, at the corner gusset plate connections. Two buckling modes were observed: a three-hinge mode involving one half of the discontinuous brace and an anti-symmetrical mode involving both segments of the discontinuous brace. The buckling mode and compressive strength were influenced by the type of connections as well as the flexural stiffness and strength of the connecting plates.

The use of an effective length of 1.2 times the mid-connection length did not permit to accurately predict the measured specimen resistances. Longer effective lengths, varying from 1.5 to 2.2, were determined from elastic stability analysis performed to account for the geometry and flexibility of the mid-connections. Improved strength predictions could be achieved when using these values together with reduced flexural stiffness properties for the connections. The proposed model showed that the properties of the mid-connections influence more the compressive strength of discontinuous braces compared to the stiffness and strength of the corner connections. Further study is needed to better define the reduced connection properties that must be used to account for inelasticity and initial imperfection effects on the brace compressive strength.

REFERENCES

AISC (2010). *ANSI/AISC 360-10, Specification for Structural Steel Buildings*. American Institute of Steel Construction (AISC), Chicago, Il.

CSA. (2009). CSA-S16-09, Design of Steel Structures, Canadian Standards Association, Willowdale, ON.

Davaran, A. 2001. Effective length factor for discontinuous X-bracing systems. *Journal of Engineering Mechanics*, ASCE, 127(2): 106-112.

Davaran, A., and Hoveidae, N. 2009. Effect of mid-connection detail on the behavior of X-bracing systems. *Journal of Construction Steel Research*, 65(4): 985-990.

Davaran, A., Gélinas, A., and Tremblay, R. (2012). “Experimental seismic response of slotted connections at the intersection of HSS braces in X-bracing systems.” *Proc. Connections VII: Seventh International Workshop on Connections in Steel Structures*, Timisoara, Romania, Paper No. 6-1.

DeWolf, J.T., and Pelliccione, J. F. (1979). “Cross-bracing design.” J. Struct. Div., ASCE, 105(7), 1379-1391.

Gélinas, A., Tremblay, R. and Davaran, A. 2012. Seismic Behavior of Steel HSS X-Bracing of the Conventional Construction Category. *Proc. Structures Congress 2012*, ASCE, Chicago, IL: 1649-1660.

Packer, J., Sherman, D., and Lecce, M. (2010). *Hollow Structural Section Connections - Steel Design Guide No. 24*, American Institute of Steel Construction (AISC), Chicago, Il.

Picard, A. and Beaulieu, D. (1987). “Design of diagonal cross-bracings. Part 1: Theoretical study.” *Eng. J.,* AISC, 24(3), 122-126.

Segal, F., Levy, R., and Rutenberg, A. (1994). “Design of imperfect cross-bracings.” *J. Engrg. Mech., ASCE*, 120(5), 1057-1075.

Stoman, S.H. (1989). “Effective length spectra for cross bracings.” *J. Struct. Eng., ASCE*, 115(12), 3112-3122.

Tremblay, R., Archambault, M.-H., and Filiatrault, A. (2003). “Seismic response of concentrically braced steel frames made with rectangular hollow bracing members.” J. Struct. Eng., ASCE, 129(12), 1626-1636.